Assessment of cavitation in artificial approximal dental lesions with near-IR imaging

Jacob C. Simon, **Cynthia L. Darling**, and **Daniel Fried**
University of California, San Francisco, San Francisco, CA 94143-0758

Abstract

Bitewing radiography is still considered state-of-the-art diagnostic technology for assessing cavitation within approximal carious dental lesions, even though radiographs cannot resolve cavitated surfaces but instead are used to measure lesion depth in order to predict cavitation. Clinicians need new technologies capable of determining whether approximal carious lesions have become cavitated because not all lesions progress to cavitation. Assessing lesion cavitation from near-infrared (NIR) imaging methods holds great potential due to the high transparency of enamel in the NIR region from λ=1300–1700-nm, which allows direct visualization and quantified measurements of enamel demineralization. The objective of this study was to measure the change in lesion appearance between non-cavitated and cavitated lesions in artificially generated lesions using NIR imaging modalities (two-dimensional) at λ =1300-nm and λ=1450-nm and cross-polarization optical coherence tomography (CP-OCT) (thee-dimensional) λ =1300-nm. Extracted human posterior teeth with sound proximal surfaces were chosen for this study and imaged before and after artificial lesions were made. A high speed dental hand piece was used to create artificial cavitated proximal lesions in sound samples and imaged. The cavitated artificial lesions were then filled with hydroxyapatite powder to simulate non-cavitated proximal lesions.

Keywords

near-IR imaging; occlusal carries; detection; reflectance; transillumination; multimodal

1. INTRODUCTION

Radiography is the main diagnostic tool for the detection and diagnosis of proximal caries (dental decay in between teeth). Cavitation is accepted as a definitive endpoint for which restoration is necessary, however cavitation cannot be determined radiographically and most proximal surfaces are not clinically accessible for visual inspection [1–4]. Studies suggest that cavitation is likely for most radiolucency's that extend into the dentin [5–8]. However, with the widespread use of fluoride, lesions have changed markedly with cavitation occurring much later and many lesions are arrested due to remineralization [3]. Radiography cannot distinguish between an active and an arrested lesion with only one measurement point [3]. It is well known that radiographs underestimate the depth of lesion penetration and the probability of cavitation depends on several factors including tooth type and the nature of the contact [1, 2, 4, 9]. Moreover, the radiographic depiction of proximal lesions is greatly influenced by the lesion shape and is often inaccurate, e.g. shallow wide lesions may appear deep while deep narrow lesions may appear shallow. Enamel manifests its highest

transparency near 1300-nm where the scattering coefficient of enamel is 20–30 times lower than it is at visible wavelengths [10, 11]. Due to the high transparency of enamel, novel imaging configurations are feasible in which the tooth can be imaged from the occlusal surface after shining light at and below the gum line, which we call occlusal transillumination [12–16]. Upon demineralization the scattering coefficient of enamel increases by 1–2 orders of magnitude at 1300-nm to yield high contrast between sound and demineralized enamel for caries detection [17]. Therefore, this wavelength range is ideally suited for the transillumination of approximal dental caries lesions. Carious lesions appear dark in transillumination images due to increased scattering and absorption by the lesion that reduces optical transmission. Approximal lesions can also be imaged in reflectance from the occlusal surface at NIR wavelengths due to the high transparency of enamel. Such lesions appear dull white compared to the transparent sound enamel. Based on that knowledge, we demonstrated the high potential of the NIR for imaging caries on both proximal and occlusal surfaces [13–15, 18, 19] and that novel imaging configurations such as occlusal transillumination and cross-polarization reflectance imaging can be used to image lesions on both occlusal and proximal surfaces [12, 15]. NIR images can be acquired from multiple perspectives to gain a more accurate depiction of the lesion. Imaging devices that can more effectively show the severity of lesions on proximal surfaces and detect cavitation should have a significant impact on the diagnosis of proximal caries.

We have carried out four prior clinical studies involving NIR transillumination imaging [15, 20, 21] and one recent study involving NIR reflectance [21]. In 2011, we carried out a clinical study of teeth with non-cavitated occlusal caries lesions that were not visible on radiographs. Teeth with suspect lesions were examined using near-IR occlusal transillumination at 1300-nm and polarization optical coherence tomography prior to restoration [15]. In a near-IR imaging clinical study completed last year, we employed three NIR imaging probes to screen for lesions on premolars scheduled for extraction, and we demonstrated that NIR image methods can achieve higher diagnostic performance than radiographs for the detection of lesions on both proximal and occlusal surfaces [21].

In previous studies we have demonstrated that OCT can be used to determine if occlusal lesions have penetrated to the underlying dentin [15] by detecting the lateral spread across the DEJ. Even though the optical penetration of NIR light can easily exceed 7-mm through sound enamel to image lesions on proximal surfaces with high contrast [22], the large increase in light scattering due to demineralization [17] typically limits optical penetration in highly scattering lesions (also dentin and bone) to 1–2 mm, thus cutting off the OCT signal before it reaches the dentinal-enamel junction (DEJ). However, most occlusal lesions rapidly spread laterally under the enamel upon contacting the more soluble softer dentin and those lesion areas under sound enamel can be readily detected with OCT. Since approximal lesions are typically located under sound enamel the same principle applies [23]. In a recent clinical study, we acquired both NIR transillumination and reflectance images and OCT images of an *in vivo* approximal clinical lesion [24].

In this pilot study, we explore the use of NIR imaging methods including NIR reflectance, NIR transillumination and optical coherence tomography for detecting lesion cavitation on simulated approximal lesions.

2. MATERIALS and METHODS

2.1 Sample Preparation

Posterior teeth with sound interproximal surfaces were selected for participation in this study. Teeth were collected from patients in the San Francisco Bay area with approval from the UCSF Committee on Human Research. The teeth were sterilized using gamma radiation and stored in 0.1% thymol solution to maintain tissue hydration and prevent bacterial growth. Samples were imaged with NIR technologies before artificial cavitated and noncavitated interproximal lesions were made. Images were acquired at sound, cavitated, and noncavitated stages. A high-speed dental hand piece and #34D diamond burr was used to drill an artificial cavitated lesion into the interproximal surface of the samples at the mesial or distal contacts. Cavitated interproximal lesions were subsequently filled with powdered hydroxyapatite and sealed with cyanoacrylate adhesive Loctite (Rocky Hill, CT) to create noncavitated artificial lesions. The grain boundaries of the hydroxyapatite powder highly scatter light in a similar fashion to the porosities in caries lesions.

2.2 NIR Occlusal Transillumination and NIR Cross-Polarized Reflectance

A high sensitivity, InGaAs, SWIR camera (SU640CSX) from Sensors Unlimited (Princeton, NJ), with a 640×512-pixel focal plane array and 12.5-μm pixel pitch was used to capture NIR cross-polarized reflectance and occlusal transillumination images of posterior teeth *in vitro*. Sample images were illuminated with filtered light from two broadband tungsten halogen lamps, E Light company (Denver, CO) delivered through independent reflectance and transillumination fiber optic cable bundles (Fig. 1). Reflectance illumination was achieved using a ring light from Volpi (Auburn, NY) equipped with a toroidal NIR linear polarizer custom made from a 3×3-inch polarizing sheet, Edmund Scientific (Barrington, NJ). Occlusal transillumination used a quadfurcated fiber optic bundle to deliver unpolarized light angled apically at the cementoenamel junction from both sides (buccal/lingual) of the tooth to illuminate interproximal regions. The near-IR camera lens system was equipped with two orthogonal linear polarizers from Thorlabs (Newtown, NJ) to produce cross-polarized reflectance images with greatly reduced specular reflection.

The outputs of both broadband light sources were filtered with optical filters housed in two motorized filter wheels, FW102 from Thorlabs. The reflectance filter wheel contained 1300-nm and 1460-nm band pass, and 1500-nm long pass filters from Spectragon (Parsippany, NJ). The occlusal transillumination filter wheel contained 1200-nm and 1500-nm long pass filters from Thorlabs. Each filter wheel also contained an aluminum disk used to block the light source providing on/off functionality to the multimodal system. Detailed schematics covering the geometry of each modality and theory of the resulting image contrast can be found in previous publications. A single axis Newport 850G actuator driven by a Newport ESP300 motion controller was utilized to focus each image in the acquisition sequence by moving the camera position. Images (12-bit) were delivered over a camera link cable to a Real Time PXIe-1071 chassis with NI-8133 embedded controller and NI-1428 frame grabber (National Instruments, Austin TX). A host computer, iMac 27-inch, Late 2015 (Apple, Cupertino, CA) running bootcamp and Windows 10 was used to control the Real Time PXIe, both filter wheels and ESP300 motion controller.

2.3 NIR Image Analysis

NIR images were analyzed using the image analysis package provided by IgorPRO software from Wavemetrics, (Lake Oswego, OR). Image line profiles 20 pixels in width were extracted from the sample across the distal/mesial margin in the buccal lingual direction for NIR reflectance and transillumination images. The line profiles were used to calculate lesion contrast based on the formulas, $(I_L–I_S)/I_L$ for reflectance and $(I_S–I_L)/I_S$ for transillumination due to their different lesion appearance. A representative value was chosen from the line profile of the lesion and sound regions. The reported contrast values can range from 0 to 1 where a 0 value represents no contrast, a 1 value represents maximum contrast, and negative values represents inverse contrast. The reported lesion contrast ranges from 0 to 1 when the lesion intensity is greater than the measured sound intensity. A negative contrast can occur when the measured sound intensity exceeds the lesion intensity and the reported values do not have a confined range. Contrast values were compared with near-IR measurements using repeated measures one-way analysis of variance (ANOVA) followed by Tukey–Kramer post-hoc multiple comparison tests using InStat statistical software (GraphPad, San Diego, CA).

2.4 Cross-polarization (CP-OCT) Optical Coherence Tomography

A cross-polarization OCT system purchased from Santec (Komaki, Aichi, Japan) was used to acquire 3D tomographic images of sound, cavitated, and noncavitated lesion stages on the samples. This system acquires only the cross-polarization image (CP-OCT), not both the cross and co-polarization images (PS-OCT). The device, Model IVS- 300-CP, utilizes a swept laser source; Santec Model HSL- 200–30 operating with a 33 kHz a-scan sweep rate. The interferometer is integrated into the handpiece which also contains the microelectromechancial (MEMS) scanning mirror and the imaging optics. This CP-OCT system can acquire complete tomographic images of a volume 6×6×7 mm in size in ~3 seconds. This system operates at a wavelength of 1,321 nm with a bandwidth of 111 nm with a measured axial resolution in air of 11.4 mm (3 dB). The lateral resolution is 80mm ($1/e^2$) with a transverse imaging window of 6×6 mm and a measured imaging depth of 7 mm in air. The polarization extinction ratio was measured to be 32 dB.

2.5 CP-OCT Image Analysis

CP-OCT scans were analyzed using software that we developed using LabView (National Instruments, Austin, TX). Tomographic images of the sample were reconstructed from the cross-polarization image. Background subtraction was carried out by subtracting the mean reflectivity of 5,000 data points measured in air from the top 100 pixels (~0.8 mm) of the 50 unprocessed a-scans (~1.0 mm) outside the sample area. The images were convolved with a Gaussian filter (3×3 filter, sigma ¼ 4) to reduce speckle noise. The 5×5 rotating kernel transformation (RKT) technique was applied in x–z and y–z spaces to emphasize thin edges while further suppressing speckle noise. B-scans were extracted from the center of the lesion, cavity or sound region or image comparison. C-scans were also used to orient the view to the location of the lesion and the extracted cross sectional images.

3. RESULTS and DISCUSSION

This study found distinct measurable differences in the appearance among sound, noncavitated approximal lesions, and cavitated approximal lesions using an artificial cavitation model imaged with near-IR (NIR) cross-polarized reflectance, transillumination and cross-polarized optical coherence tomography (CP-OCT). NIR cross-polarized reflectance and occlusal transillumination imaging modalities were capable of imaging different dental lesion states at multiple wavelengths throughout the NIR spectral region (Table 1). The measured lesion contrast from line profiles extracted from regions across the lesion structure demonstrated statistically higher values for noncavitated lesions than lesions post cavitation with high significance at all tested NIR wavelengths. Figure 2 is an array of multispectral NIR images acquired in this study from a representative sample. The noncavitated lesion is visible in high contrast for all imaging wavelengths and modalities. At this stage the lesion is observed in highest contrast in reflectance at 1460-nm and at 1500-nm, and previous studies have demonstrated that these regions yield similar contrast values (for this reason they are grouped into one category in Table 1). Surprisingly, and possibly due to the "severity" of the artificial lesion, the occlusal transillumination at wavelengths coincident with increased water absorption, λ=1500–1700-nm, performed remarkably well yielding clear images of the approximal lesions.

In the cavitated state, the contrast measured in the respective cavitated areas was either not detectable, or increased, i.e. the area appeared brighter that the surrounding sound tissue due to the vacancy in the cavity (n=2). This behavior explains the negative contrast values reported in Table 1. The cavitated lesions were still evident in the reflectance images coincident with high water absorption, but the contrast was greatly reduced relative to the noncavitated state (23.5 difference in mean contrast). Reflectance images at λ=1300 demonstrated improved potential compared to λ=1500–1700 in recognizing lesion cavitation. At this stage the lesion areas were barely detectable in the cavitated images (Fig. 2K) and the loss of signal in the NIR reflectance image at λ=1300 may be a reliable indicator of active cavitation.

The results from the NIR reflectance and transillumination images in this study of artificial cavities suggest that there are distinct and detectable changes in lesion contrast that could indicate the cavitation state of active lesions. This approach would require monitoring the lesion contrast of active lesions over time using multispectral multimodal probes as the method relies on detecting changes in the lesion appearance, ie a significant loss in contrast and possible negative contrast in transillumination.

Figure 3 shows 3D CP-OCT images acquired from the sample shown in Fig. 2. The left column of Fig. 3 shows the occlusal surface of the tooth (c-scan) in the sound, noncavitated lesion, and cavitated lesion states. In Figs. 3 D & G the lesion is highlighted in red and the occlusal surface is shown in blue. The middle and right columns show b-scan cross sections extracted from the mesiodistal (vertical) and faciolingual (horizontal) yellow lines in the respective c-scan image. In the CP-OCT b-scans, the presence of a noncavitated lesion and cavitated lesion is clearly seen. Figure 3E manifests high scattering at the surface of the lesion with increased signal intensity extending into the body of the decay in both axes. In

the cavitated images (Fig. 3H & I) there is a detectable signal at the surface of the cavity due to the interface. The signal is less intense and there is no signal from the underlying void till the bottom of the cavity is detected which is indicated by the bottom arrow in Fig. 3 H.

Acknowledgments

References

1. Pitts NB, Rimmer PA. An in vivo comparison of radiographic and directly assessed clinical caries status of posterior approximal surfcaes in primary and permanent teeth. Caries Res. 1992; 26:146–152. [PubMed: 1521308]

2. Zandona, AG Ferreira, Analoui, M., Beiswanger, BB., Isaacs, RL., Kafrawy, AH., Eckert, GJ., Stookey, GK. An in vitro comparison between laser fluorescence and visual examination for detection of demineralization in occlusal pits and fissures. Caries Res. 1998; 32(3):210–8. [PubMed: 9577987]

3. Wenzel A. Bitewing and digital bitewing radiography for detection of caries lesions. J Dent Res. 2004; 83(Spec No C):C72–5. [PubMed: 15286126]

4. Wenzel A. Radiographic display of carious lesions and cavitation in approximal surfaces: Advantages and drawbacks of conventional and advanced modalities. Acta Odontol Scand. 2014; 72(4):251–64. [PubMed: 24512205]

5. Eli I, Weiss EI, Tzohar A, Littner MM, Gelernter I, Kaffe I. Interpretation of bitewing radiographs. Part 1. Evaluation of the presence of approximal lesions. J Dent. 1996; 24(6):379–83. [PubMed: 8990680]

6. Weiss EI, Tzohar A, Kaffe I, Littner MM, Gelernter I, Eli I. Interpretation of bitewing radiographs. Part 2. Evaluation of the size of approximal lesions and need for treatment. J Dent. 1996; 24(6): 385–8. [PubMed: 8990681]

7. Mejare I, Malmgren B. Clinical and radiographic appearance of proximal carious lesions at the time of operative treatment in young permanent teeth. Scand J Dent Res. 1986; 94(1):19–26. [PubMed: 3458277]

8. Hintze H, Wenzel A, Danielsen B, Nyvad B. Reliability of visual examination, fibre-optic transillumination, and bite-wing radiography, and reproducibility of direct visual examination following tooth separation for the identification of cavitated carious lesions in contacting approximal surfaces. Caries Res. 1998; 32(3):204–9. [PubMed: 9577986]

9. Fejerskov, O., Kidd, E. Dental Caries: The Disease and its Clinical Management. Blackwell; Oxford: 2003.

10. Fried D, Featherstone JDB, Glena RE, Seka W. The nature of light scattering in dental enamel and dentin at visible and near-IR wavelengths. Appl Optics. 1995; 34(7):1278–1285.

11. Jones RS, Fried D. Attenuation of 1310-nm and 1550-nm Laser Light through Sound Dental Enamel. Lasers in Dentistry VIII. Proc SPIE. 2002; 4610:187–190.

12. Buhler C, Ngaotheppitak P, Fried D. Imaging of occlusal dental caries (decay) with near-IR light at 1310-nm. Optics Express. 2005; 13(2):573–82. [PubMed: 19488387]

13. Fried D, Featherstone JDB, Darling CL, Jones RS, Ngaotheppitak P, Buehler CM. Early Caries Imaging and Monitoring with Near-IR Light. Dental Clinics of North America - Incipient and Hidden Caries. 2005; 49(4):771–794.

14. Hirasuna K, Fried D, Darling CL. Near-IR imaging of developmental defects in dental enamel. J Biomed Opt. 2008; 13(4):044011:1–7. [PubMed: 19021339]

15. Staninec M, Lee C, Darling CL, Fried D. In vivo near-IR imaging of approximal dental decay at 1,310 nm. Lasers Surg Med. 2010; 42(4):292–8. [PubMed: 20432277]

16. Lee C, Lee D, Darling CL, Fried D. Nondestructive assessment of the severity of occlusal caries lesions with near-infrared imaging at 1310 nm. J Biomed Opt. 2010; 15(4):047011. [PubMed: 20799842]

17. Darling CL, Huynh GD, Fried D. Light Scattering Properties of Natural and Artificially Demineralized Dental Enamel at 1310-nm. J Biomed Optics. 2006; 11(3):1–11. 034023.

18. Bühler CM, Ngaotheppitak P, Fried D. Imaging of occlusal dental caries (decay) with near-IR light at 1310-nm. Lasers in Dentistry XI SPIE. 2005; 5687:125–131.

19. Jones RS, Huynh GD, Jones GC, Fried D. Near-IR Transillumination at 1310-nm for the Imaging of Early Dental Caries. Optics Express. 2003; 11(18):2259–2265. [PubMed: 19466117]

20. Staninec M, Douglas SM, Darling CL, Chan K, Kang H, Lee RC, Fried D. Nondestructive Clinical Assessment of Occlusal Caries Lesions using Near-IR Imaging Methods. Lasers Surg Med. 2011; 43(10):951–959. [PubMed: 22109697]

21. Simon JC, Lucas SA, Lee RC, Staninec M, Tom H, Chan KH, Darling CL, Fried D. Near-IR Transillumination and Reflectance Imaging at 1300-nm and 1500–1700-nm for in vivo Caries Detection. Lasers Surg Med. 2016; 48(6):828–836. [PubMed: 27389018]

22. Jones G, Jones RS, Fried D. Transillumination of interproximal caries lesions with 830-nm light. Lasers in Dentistry X SPIE. 2004; 5313:17–22.

23. Ngaotheppitak P, Darling CL, Fried D. Measurement of the severity of natural smooth surface (interproximal) caries lesions with polarization sensitive optical coherence tomography. Lasers Surg Med. 2005; 37(1):78–88. [PubMed: 15889402]

24. Simon JC, Kang H, Staninec M, Jang AT, Chan KH, Darling CL, Lee RC, Fried D. Near-IR and CP-OCT imaging of suspected occlusal caries lesions. Lasers Surg Med. 2017 In Press.
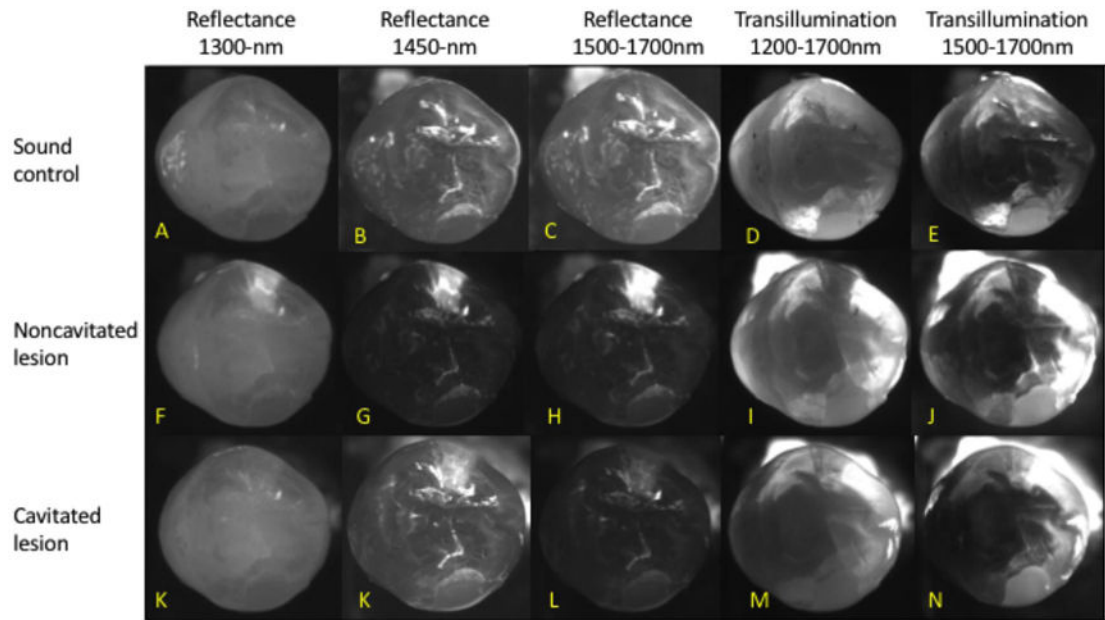
Fig 1.
Imaging schematic for multispectral-multimodal NIR reflectance and occlusal transillumination system. Solid black lines represent fiber optic bundles. Black arrows represent data communication and control. (A) SU640CSX InGaAs NIR camera. (B) NIR linear polarizer. (C) Single axis focusing stage (850G Actuator). (D) Reflectance ring light. (E) Toroidal linear polarizer. (F) Unpolarized occlusal transillumination lights (2 of 4 illustrated). (G) Filter wheel (1 of 2 illustrated).

Fig. 2.
Multispectral NIR cross-polarized reflectance and occlusal transillumination images of sound, noncavitated lesion and cavitated lesions.
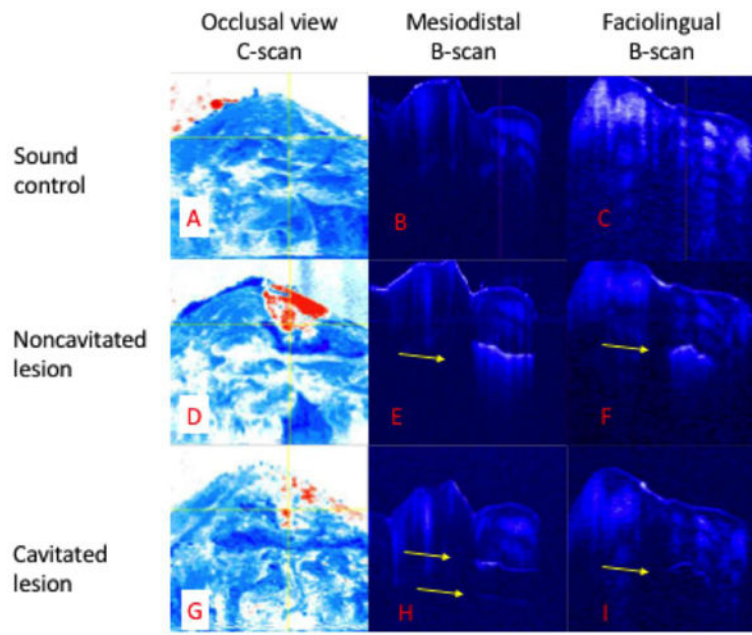
Fig. 3.
CP-OCT Images of sound, noncavitated, and cavitated lesion states of the sample in Fig. 2. Panels A,D & E are c-scan OCT images of the occlusal surface and should be compared with the reflectance images in Fig.2. The lesion is shown in red. Vertical yellow line corresponds to mesiodistal b-scan (B,E & H). Horizontal yellow line correspond with facioligual b-scan (C,F & I).

Table 1

The mean lesion contrast measure for image line profiles extracted from NIR reflectance and transillumination images at difference lesion stages.

Means and Difference of Means in NIR image contrast before and after Cavitation		Noncavitated Lesion Mean (SD)	Cavitated Lesion Mean (SD)	Difference of Means
Cross -polarized Reflectance Wavelength	1300-nm n =8	37.3 (8.5)	7.2 [*] (4.2)	30.1
	1460–1700-nm n =10	62.8 (15.4)	39.3 [*] (10.9)	23.5
Transillumination Wavelength	1200–1700-nm n =4	30.1 (21.4)	0 [*] (0)	30.1
	1500–1700-nm n =6	39.6 (22.4)	−12.3 [*] (19.9)	51.9

[*] The decrease in lesion contrast upon cavitation of the artificial lesions was statistically significant (P<0.05) for each modality.